A Centralized MINLP-based MPC for Building Microgrid with Surface Water Heat Pump*

Nassima Ouali, Thomas Chevet, and Nicolas Langlois

***Abstract*—Buildings have attracted the European Union's interest as there is a need to improve their energy consumption. Current efforts emphasize sustainable heating solutions based on aquathermal renewable energy through the WaterWarmth project. This paper presents an energy management strategy for building microgrids. The aim is to manage microgrid energy flows in order to reduce energy consumption while ensuring occupant thermal comfort within the building. The considered energy system consists of PV generation, grid energy exchanges, and a battery energy storage. A surface water heat pump (SWHP) coupled with a thermal buffer tank is used to improve energy efficiency while meeting the building heating demand. A centralized model predictive control strategy is proposed. The resulting optimization problem is formulated as a mixed-integer nonlinear programming model that explicitly incorporates the nonlinear dynamics and operational constraints of the system. The building microgrid is optimized based on multiple factors, including weather conditions, electricity prices and surface water temperature. The results show that the proposed approach effectively manages energy flow in the microgrid, while the SWHP operates at $25\,\%$ of its nominal power and maintains a stable buffer tank temperature. The control strategy also ensures indoor thermal comfort with the heating system operating at approximately $30\,\%$ of its nominal power.**

***Index Terms*—Surface water heat pump, Renewable energy, Microgrid, Model predictive control, Mixed integer nonlinear programming**

I. Introduction

In Europe, the rapid trend of urbanization contributes to significant construction activities. Buildings in both residential and tertiary sectors accounted for around $30\,\%$ of the global final energy consumption in 2023, a large share of this energy consumed by heating systems, thus constituting $26\,\%$ of gas emissions [1]. Growing concerns about global warming have led to increased efforts to reduce carbon emissions and dependence on fossil fuels, supported by the European Union. This transition is driven by the increasing integration of renewable energies including solar and aquathermal energy sources, surface water heat pump (SWHP), and energy storage technologies to increase self-consumption and reduce grid electricity consumption in building microgrids (BMGs) [2], [3].

The widespread use of low stable energy powered heat pumps for BMGs has been enabled by recent technological developments [4]. The heat pump operates by extracting heat from a low-temperature source using a refrigerant which is then compressed, thus increasing its temperature and pressure. After that it releases heat to a high-temperature sink. The cycle is closed, an expansion process returning the fluid to its original temperature. In particular, SWHPs are progressively integrated into BMG systems owing to their capability for significant energy savings by using natural water resources. SWHPs use stable thermal water bodies, namely surface water, groundwater, or wastewater as heat sources or sinks to meet building heating demands via the refrigeration cycle. Moreover, their coefficient of performance (COP) is generally higher than that of air source heat pumps, providing greater operational flexibility. Consequently, the integration of aquathermal energy enables highly efficient clean energy heating in BMGs, while SWHP have emerged as a promising technology for low carbon and sustainable energy use [5].

The increasing complexity of the BMGs integrating SWHP and heating systems involves advanced energy management strategy (EMS), where sophisticated control algorithms are essential. Model predictive control (MPC) has been extensively studied as a promising method for achieving BMGs efficiency and energy saving compared to traditional control methods, such as proportional integral derivative controllers or rule-based control methods, which are insufficient to adapt to changing in system states and multiple operating conditions of the BMGs [6]. Moreover, their fixed control laws limit the use of prediction information, as in predicted weather variations. MPC uses a mathematical model to forecast the behavior of the BMG in response to varying operating conditions and energy demands. Furthermore, it incorporates an optimization algorithm to fit an optimal control sequence over a finite prediction horizon while considering system constraints [7], [8]. Several MPC implementations in BMGs have shown a potential for energy savings [9]–[11]. Nevertheless, many of these studies rely on simplified or linearized representations of system dynamics that do not fully capture the behavior of highly nonlinear and dynamic behavior of the BMGs. Besides, these simplifications generally lead to linear formulation of the optimization problem that do not account for actuator limits and system constraints within the control design [12]. To overcome this challenge, a centralized model predictive control (C-MPC) based on solving complex multi-objective optimization problems is proposed.

In this paper, the BMG consists of PV generation, grid exchanges,a battery energy storage system (BESS) and a SWHP coupled with thermal energy storage (TES) supplying the building to be heated. The building model is based on a resistance-capacitance (RC) model to capture the building

*This work was supported by the Interreg North Sea program, co-funded by the European Union, through the WaterWarmth project.

The authors are with Univ Rouen Normandie, ESIGELEC, Normandie Univ, IRSEEM UR4353, F-76000 Rouen, France <first name>.<last name>@irseem-esigelec.fr

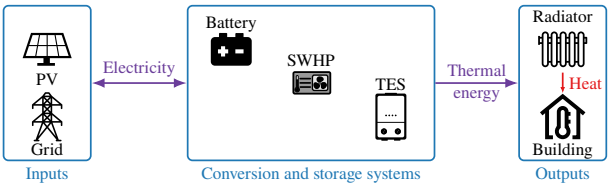

Fig. 1. Building microgrid architecture.

thermal dynamics. The objective of the proposed centralized MPC strategy is to optimize energy flows in the BMG while ensuring the indoor occupant comfort, under all operational constraints of the subsystems [13]. Furthermore, the BMG is compounded by external factors such as forecasted weather conditions (solar radiation and external temperature, surface water temperature), ambient temperature of the technical TES room and variable time-of-use electricity tariffs from the grid [14]. Thus, the optimization problem is formulated as mixed integer non-linear program (MINLP) [15] explicitly incorporating nonlinear system dynamics and operational constraints providing a relatively accurate representation of the BMG subsystems. The main contributions of this paper can be summarized as follows

- the dynamic coefficient of performance (COP) of the SWHP is incorporated into the prediction model to improve accuracy;
- the dynamic buffer tank TES losses are considered within the prediction model;
- a centralized MINLP-based MPC strategy is proposed to handle the nonlinear dynamics and operational constraints of the BMG control problem.

This paper is organized as follows. Section II presents the description of the building microgrid with its dynamic modelling. Section III addresses the control problem and proposes a solution based on MINLP. Section IV discusses the main results obtained. Finally, conclusions are drawn in Section V.

II. BMG SYSTEM DESCRIPTION AND MODELLING

The BMG integrates renewable resources, including PV generation and SWHP. Figure 1 illustrates the electrical and thermal energy flows exchanged through a common electrical bus in the BMG. The PV supplies electricity to the SWHP, while surplus is either stored in the BESS or delivered to the grid through bidirectional power exchanges. The SWHP operates as an energy conversion system within the energy hub [16] by using electrical energy obtained from the BESS, which is charged with the excess PV production or purchased from the grid when the battery is not used, to extract heat from the surface water source. The generated thermal energy is then delivered to the TES. The TES serves as both a thermal storage and buffer tank unit which ensures a stable heat supply for the hydronic heating system in the building.

For the design of the BMG and its control strategy, we describe the main dynamical equations characterizing the thermal and electrical energy systems.

A. BMG's thermal models

The SWHP constitutes the core conversion system of the energy hub and is connected to the buffer tank. It extracts thermal energy from a surface water source and elevates its temperature to a higher level, then converting electrical energy into heat with

$$Q_{\text{SWHP}}(t) = \text{COP}_{\text{H}}(t) P_{\text{SWHP}}(t) \tag{1}$$

where $Q_{\text{SWHP}}(t)$ and $P_{\text{SWHP}}(t)$ represent the thermal power delivered by the heat pump and its electrical power consumption, respectively. $\text{COP}_{\text{H}}(t)$ is the coefficient of performance which reflects the thermodynamic efficiency of a heat pump system. The SWHP performance is highly dependant on the surface water and supply temperatures, which allows accurate estimation of the heat pump COP as

$$\text{COP}_{\text{H}}(t) = \alpha_1 + \alpha_2 (T_{\text{B_tank}}(t) - T_{\text{sw}}(t)) \tag{2}$$

where $T_{\text{B_tank}}(t)$ denotes the temperature of the buffer tank and $T_{\text{sw}}(t)$ the surface water temperature.

In this paper, the TES is modelled by the dynamic evolution of the buffer tank temperature. In addition, thermal losses through the tank walls are considered as a function of the temperature difference between the buffer tank and the surrounding technical room where the TES is installed [17], expressed by

$$Q_{\text{loss}}(t) = k_{\text{B}} (T_{\text{B_tank}}(t) - T_{\text{a}}(t)) \tag{3}$$

where k_{B} is the heat loss from the buffer tank and T_{a} the ambient temperature of the technical room. Thus, the energy balance equation of the buffer tank is

$$C_w m \frac{\text{d}T_{\text{B_tank}}}{\text{d}t} = Q_{\text{SWHP}}(t) - Q_{\text{H_dem}}(t) - Q_{\text{loss}}(t) \tag{4}$$

where C_w denotes the specific heat capacity of water and m its mass in the tank, while $Q_{\text{H_dem}}(t)$ represents the heating demand of the residential building. This demand is satisfied by a hydronic radiator system connected to the TES [17], so that

$$Q_{\text{H_dem}}(t) = k_{\text{H}} u_{\text{H}}(t) (T_{\text{B_tank}}(t) - T_{\text{in}}(t)) \tag{5}$$

where k_{H} is the heat transfer coefficient between the buffer tank and the heating system within the building, $u_{\text{H}}(t)$ the heating control input, and $T_{\text{in}}(t)$ the temperature inside the building. This work uses simple 1R1C low-order thermal dynamic models, based on electrical circuits analogy. The model requires only a minimal set of information of the building to describe heat transfer dynamics as illustrated in Figure 2.

The circuit, defined by its thermal resistance and thermal capacitance, provides a simplified effective representation of the building's energy behavior [18], [19]. The model characterizes indoor temperature dynamics, capturing the building's thermal inertia and allowing its use to provide energy demand in response to the outdoor temperature T_{o} and heating power control signal u_{H}. It is given by

$$C_H \frac{\text{d}T_{\text{in}}}{\text{d}t} = Q_{\text{H_dem}}(t) - L_H (T_{\text{in}}(t) - T_{\text{o}}(t)) \tag{6}$$

where $L_H = 1/R_H$ and C_H denote the thermal transmittance and thermal capacitance of the building, respectively.

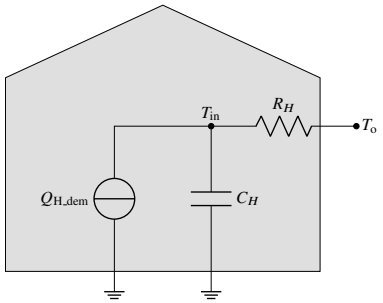

Fig. 2. RC building model.

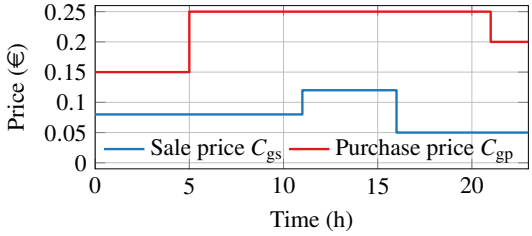

Fig. 3. Grid electricity price.

B. BMG's electrical models

Regarding the electrical energy, the battery is considered first. The state of charge represents the energy stored in the battery and is governed by the battery's charging and discharging dynamic behavior

$$E_{\mathrm{B}} \frac{\mathrm{dSOC_B}}{\mathrm{d}t} = \eta_{\mathrm{ch}} P_{\mathrm{B_ch}}(t) - \eta_{\mathrm{dis}} P_{\mathrm{B_dis}}(t) \tag{7}$$

where η_{ch} and η_{dis} represent the charging and discharging efficiencies, respectively, $P_{\mathrm{B_ch}}$ and $P_{\mathrm{B_dis}}$ denote the battery charging and discharging power and E_{B} is the nominal energy capacity of the battery.

Regarding the PV system, its generated power is represented by a simplified efficiency model that depends on solar irradiance

$$P_{\mathrm{PV}} = \eta_{\mathrm{PV}} A_{\mathrm{PV}} I_{\mathrm{solar}} \tag{8}$$

where P_{PV} is the PV generated power, A_{PV} and I_{solar} denote the PV panel area and solar irradiance measurement, respectively, and η_{PV} is the PV efficiency .

We also consider the electricity exchanges with the grid to cover the full electrical demand. The main grid is modelled as a bidirectional power exchange interface with finite import and export capacities, and are determined by a time of use pricing scheme, as shown in Figure 3. Electricity is purchased when PV generation and battery power are insufficient to meet the demand and any surplus PV electricity is sold to the grid.

III. Control Problem Definition

The primary objective of the proposed C-MPC based EMS is to manage energy flows in the BMG in order to achieve efficient energy saving with higher indoor comfort. The C-MPC uses forecasts of grid electricity prices and weather conditions (irradiance and outdoor temperature), as well as the temperature of surface water and the ambient temperature of the technical room. The objective is formulated as a multi objective approach that ensures the economical use of grid and limits battery degradation. The tank buffer is also adjusted to track a reference temperature in order to provide a stable heat supply to the building. Another objective is to maintain the building occupants' thermal comfort at the desired level. Accordingly, the cost function used is

$$\begin{aligned} J_{\text{C-MPC}}(k) = \sum_{i=k}^{k+N_{\mathrm{p}}-1} \Big(& C(i) P_{\mathrm{grid}}(i) \\ & + \delta_{B1} P_{\mathrm{B_dis}}(i) - \delta_{B2} P_{\mathrm{B_ch}}(i) \\ & + \delta_{\mathrm{B_tank}} \left(T_{\mathrm{B_tank}}(i) - T_{\mathrm{f}}(i) \right)^2 \\ & + \delta_P \left(T_{\mathrm{in}}(i) - T_{\mathrm{sp}}(i) \right)^2 \Big). \end{aligned} \tag{9}$$

The goal is to minimize the cost function at each sampling time over the prediction horizon N_{p}. C is the vector of grid electricity prices, defined as $C(i) = \begin{bmatrix} C_{\mathrm{gp}}(i) & \mathrm{C_{gs}}(i) \end{bmatrix}^\top$ with C_{gp} and C_{gs} the grid electricity purchase and selling prices, respectively. P_{grid} represents the power exchanged with the grid, defined as $P_{\mathrm{grid}}(i) = \begin{bmatrix} P_{\mathrm{gp}}(i) & \mathrm{P_{gs}}(i) \end{bmatrix}^\top$ where P_{gp} and P_{gs} denote the power purchased and sold from the grid, respectively. T_{f} is the temperature reference of the buffer tank, while T_{sp} is the desired building temperature. $\delta_{\mathrm{B_tank}}$, δ_{B1} ,δ_{B2}, δ_P are weighting factors. To control the system using the C-MPC scheme, the BMG dynamics and operational constraints are taken into account. To ensure power balance, the BMG energy system follows, at time k and for any $i \in \{k, k+1, \ldots, k+N_{\mathrm{p}}\}$,

$$P_{\mathrm{PV}}(i) + P_{\mathrm{gp}}(i) + P_{\mathrm{B_dis}}(i) = P_{\mathrm{gs}}(i) + P_{\mathrm{B_ch}}(i) + P_{\mathrm{SWHP}}(i) \tag{10}$$

where the PV power $P_{\mathrm{PV}}(i)$ is constrained by the available PV generation $P_{\mathrm{pv_real}}(i)$, as

$$0 \leq P_{\mathrm{PV}}(i) \leq P_{\mathrm{pv_real}}(i). \tag{11}$$

The electrical power of the SWHP power is also limited to its maximum power $\bar{P}_{\mathrm{SWHP}}$

$$0 \leq P_{\mathrm{SWHP}}(i) \leq u_{\mathrm{SWHP}}(i) \bar{P}_{\mathrm{SWHP}} \tag{12}$$

where $u_{\mathrm{SWHP}}(i) \in [0, 1]$ is the continuous control variable of the SWHP. The battery charging and discharging power are constrained with respective minimum and maximum power operating limits as

$$0 \leq P_{\mathrm{B_ch}}(i) \leq u_{\mathrm{ch}}(i) \bar{P}_{\mathrm{B_ch}} \tag{13a}$$

$$0 \leq P_{\mathrm{B_dis}}(i) \leq u_{\mathrm{dis}}(i) \bar{P}_{\mathrm{B_dis}} \tag{13b}$$

where $\bar{P}_{\mathrm{B_ch}}$ and $\bar{P}_{\mathrm{B_dis}}$ denote the maximum battery charging power and maximum battery discharging power, respectively, and $u_{\mathrm{ch}}(i), u_{\mathrm{dis}}(i) \in \{0, 1\}$ are binary control variables for battery charging and discharging, respectively. As the battery cannot be charged and discharged at the same time,

$$u_{\mathrm{ch}}(i) + u_{\mathrm{dis}}(i) \leq 1. \tag{14}$$

Similarly, the grid electricity purchase and selling power are constrained with respective minimum and maximum power operating limits as

$$0 \leq P_{\text{gp}}(i) \leq u_{\text{gp}}(i)\bar{P}_{\text{gp}} \tag{15a}$$
$$0 \leq P_{\text{gs}}(i) \leq u_{\text{gs}}(i)\bar{P}_{\text{gs}} \tag{15b}$$

where $\bar{P}_{\text{gp}}$ and $\bar{P}_{\text{gs}}$ denote the maximum power purchased from the grid and the maximum power sold to the grid, respectively, and $u_{\text{gp}}(i), u_{\text{gs}}(i) \in \{0,1\}$ are binary control variables for grid purchasing and selling, respectively. As the microgrid cannot buy from and sell the electricity to the grid at the same time,

$$u_{\text{gp}}(i) + u_{\text{gs}}(i) \leq 1. \tag{16}$$

To ensure stable operation of the BESS and buffer tank TES, safety ranges are defined as

$$\underline{\text{SOC}}_{\text{B}} \leq \text{SOC}_{\text{B}} \leq \overline{\text{SOC}}_{\text{B}} \tag{17}$$
$$\underline{T}_{\text{B_tank}} \leq T_{\text{B_tank}} \leq \bar{T}_{\text{B_tank}} \tag{18}$$

where $\underline{\text{SOC}}_{\text{B}}$ and $\overline{\text{SOC}}_{\text{B}}$ are the lower and upper limit of SOC_{B} values, respectively, while $\underline{T}_{\text{B_tank}}$ and $\bar{T}_{\text{B_tank}}$ are lower and upper limit of $T_{\text{B_tank}}$, respectively.

The discrete control variables of the battery and grid subsystems $u_{\text{ch}}(i), u_{\text{dis}}(i), u_{\text{gp}}(i), u_{\text{gs}}(i)$, combined with the continuous control inputs of the SWHP $u_{\text{SWHP}}(i)$ and of the heating system $u_{\text{H}}(i)$ make the control problem a mixed integer program.

The dynamics of the controlled system can be written, at time k, and for any $i \in \{k, k+1, \ldots, k+N_{\text{p}}-1\}$, as

$$x_{\text{BMG}}(i+1) = g(x_{\text{BMG}}(i), u_{\text{BMG}}(i), z_{\text{BMG}}(i)) \tag{19}$$

where (19) captures the dynamic of BMG representing the buffer tank state, the battery state of charge and the indoor temperature of the building. In these dynamics, $x_{\text{BMG}} = \begin{bmatrix} T_{\text{B_tank}} & SOC_{\text{B}} & T_{\text{in}} \end{bmatrix}^\top$ is the BMG's state, $u_{\text{BMG}} = \begin{bmatrix} u_{\text{SWHP}} & u_{\text{H}} & P_{\text{grid}}^\top & P_{\text{B_ch}} & P_{\text{B_dis}} \end{bmatrix}^\top$ its continous control variables, and $z_{\text{BMG}} = \begin{bmatrix} u_{\text{ch}} & u_{\text{dis}} & u_{\text{gp}} & u_{\text{gs}} \end{bmatrix}^\top$ its binary control variables, while g is obtained by discretizing equations (4), (6), and (7) (using also the algebraic relations (1), (2), (3) and (5)) with sampling period T_{s}.

The optimization problem to be solved is then formulated, at time k, as

$$\min_{\substack{u_{\text{BMG}}(i), z_{\text{BMG}}(i), \\ i \in \{k, k+1, \ldots, k+N_{\text{p}}-1\}}} \quad J_{\text{C-MPC}}(k) \tag{20a}$$

s.t.

$$(8), (10), (11), (12), (13), (14), (15), (16), (17), (18), (19),$$
$$\text{for } i \in \{k, k+1, \ldots, k+N_{\text{p}}-1\}. \tag{20b}$$

IV. Simulation Results

To evaluate the effectiveness of the proposed centralized MPC strategy, optimization problem (20) is solved at each sampling time, with $T_{\text{s}} = 900\,\text{s}$, over a prediction horizon of 1 hour (that is $N_p = 4$). The weighting parameters are selected to allow the C-MPC controller to achieve a suitable trade-off between the different BMG objectives. In this simulation, δ_{B1} and δ_{B2} are set to 0.18 and 0.1, respectively, in order to ensure an efficient battery charge and discharge cycle while limiting battery degradation. In addition, $\delta_{\text{B_tank}}$ is set to 10 and δ_P to 20 to ensure temperature tracking performance and meet the building demand. The APOPT solver, integrated into the GEKKO Python library [20], is used as it is a MINLP solver, and the different thermal and electrical parameters used in simulation are indicated in Tables I and II.

TABLE I
Thermal parameters used for the simulations

Thermal parameters	Value
C_H, L_H	$1.2\,\text{MJ}/^\circ\text{C}$, $33\,\text{W}/^\circ\text{C}$
k_{B}, k_{H}	$3\,\text{W}/^\circ\text{C}$, $40\,\text{W}/^\circ\text{C}$
C_w	$4186\,\text{J}/(\text{kg}\cdot^\circ\text{C})$
m	$150\,\text{kg}$
$\underline{T}_{\text{tank}}$, $\bar{T}_{\text{tank}}$	$30\,^\circ\text{C}$, $60\,^\circ\text{C}$
α_1, α_2	4.7, $-0.046/^\circ\text{C}$

TABLE II
Electrical parameters used for the simulations

Electrical parameters	Value
E_{B}	$3\,\text{kW}\cdot\text{h}$
$\bar{P}_{\text{B_ch}}$, $\bar{P}_{\text{B_dis}}$	$0.8\,\text{kW}$, $0.8\,\text{kW}$
η_{ch}, η_{dis}	0.95, 0.85
$\bar{P}_{\text{SWHP}}$	$0.7\,\text{kW}$
A_{PV}	$20\,\text{m}^2$
$\bar{P}_{\text{gp}}$, $\bar{P}_{\text{gs}}$	$1\,\text{kW}$, $1\,\text{kW}$

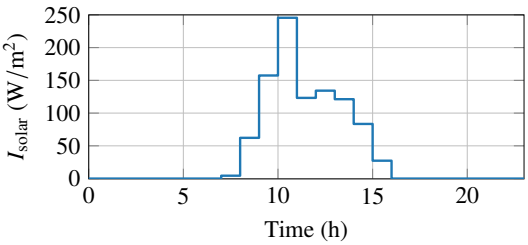

Fig. 4. Solar irradiance for November 23, 2025, in Ouistreham.

Figures 4 and 5 indicate the measured outdoor temperature and solar irradiance profiles throughout the day of November 23, 2025, collected around a pilot site of the WaterWarmth project [21] located in Ouistreham, Normandie, France [22]. In addition, Figure 6 shows the considered external conditions, including the surface water temperature and the ambient temperature in the TES equipment room. The results illustrate the dynamic behavior of BMG.

Figure 7 shows the heat pump control signal. At the beginning of the simulation, the SWHP operates at its full capacity to increase the temperature of the buffer tank. After approximately 3 hours, the heat output of the SWHP is

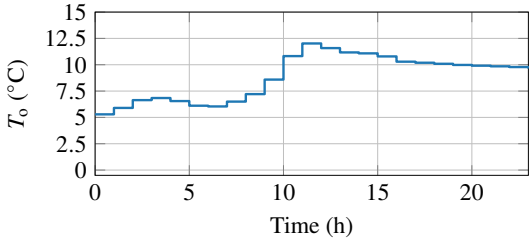

Fig. 5. Outdoor temperature for November 23, 2025, in Ouistreham.

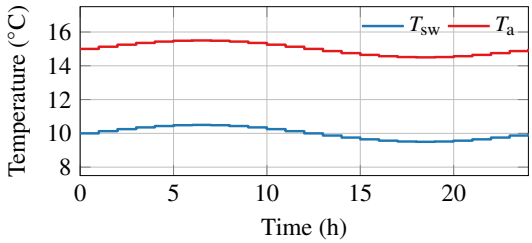

Fig. 6. External temperatures

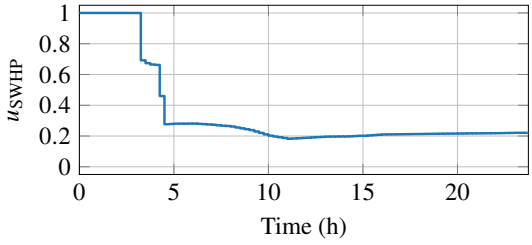

Fig. 7. Surface water heat pump control signal.

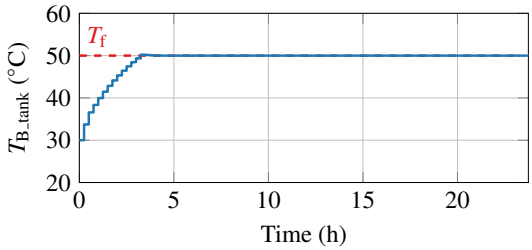

Fig. 8. Buffer tank thermal storage temperature.

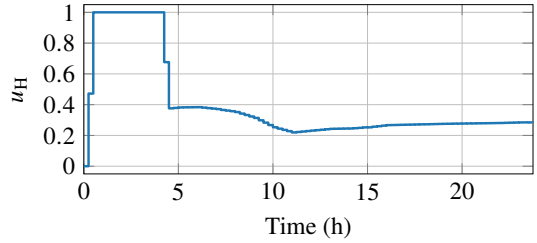

Fig. 9. Heating control signal.

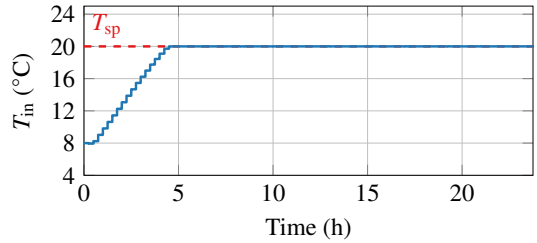

Fig. 10. Indoor temperature inside the building.

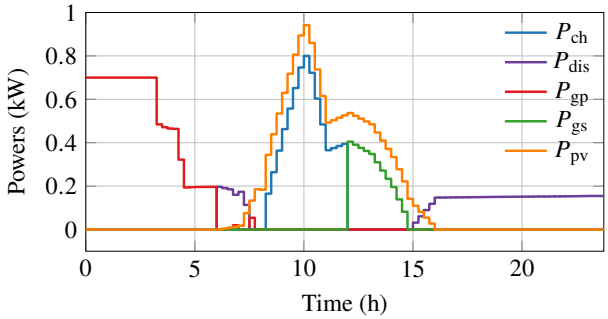

Fig. 11. Electrical power flows from and to the grid and battery charging profile.

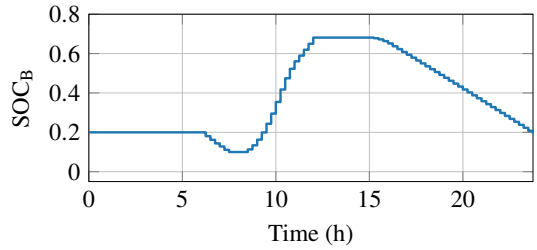

Fig. 12. Battery state of charge.

adjusted to maintain a stable buffer tank temperature T_{B_tank}. Consequently, the T_{B_tank} reaches and accurately tracks the reference temperature of 50 °C, despite the heat losses of TES, as shown in Figure 8. Meanwhile, the SWHP control signal gradually decreases to operate at 25 % of its nominal power and then remains nearly constant throughout the day, despite variations in the COP_H due to the change in system state and the surface water temperature T_{sw}.

Figure 9 indicates the heating system control signal. It can be observed that the heating system is activated after a few minutes of the operation of SWHP. Then, it operates at full power to maintain the indoor temperature at the desired temperature. The indoor temperature gradually increases until it reaches 20 °C and stays stable through the day ensuring occupant thermal comfort in the building as shown in Figure 10 despite the building heat losses to the outdoor environment. Consequently, the hydronic heating system operates at a reduced power level, approximately 30 % of its nominal power. This behavior confirms the effective thermal interaction between the buffer tank and the hydronic heating system in meeting the building heating demand under varying outdoor temperature conditions.

Figure 11 and Figure 12 illustrates the energy exchanges and battery state of charge within the microgrid in response to the building demand, respectively. At midnight, the building demand is fully supplied by the grid, with a maximum imported power $P_{\text{gp}}(i)$ of approximatively $700\,\text{W}$. After a few hours, $P_{\text{gp}}(i)$ gradually decreases as the demand is relatively satisfied while the battery remains inactive due to the absence of PV generation. Around 5 a.m. as PV generation starts, grid imports decrease to $0\,\text{W}$ and the battery briefly supports the demand, which causes a slight drop in its SOC_B to the minimum limit of 0.1. During the day, the solar irradiance increases and exceeds the required demand, so SOC_B rises within its operational limits, with surplus PV energy charging the battery up to $800\,\text{W}$ and exporting up to $400\,\text{W}$ to the grid. At the night, the stored energy is used to supply the load, thus leading to a gradual decrease in SOC_B. These results, demonstrate an effective coordination of the SWHP, PV generation, and BESS, resulting in high PV self-consumption and reduced grid electricity imports while meeting the building demand and respecting operational constraints.

V. Conclusion

This paper presented a centralized energy management strategy for building microgrids. The aim is to ensure effective management of energy flows between electrical and thermal energies, reduce energy use and maintain occupant comfort. The integration of surface water heat pump with the PV and grid electricity usage combined with energy storages increase the operational complexity of BMGs. To address these complexities and meet BMG objectives, a mixed-integer nonlinear-based centralized model predictive control (MINLP-based C-MPC) strategy was designed. The proposed optimization approach accounts for both the nonlinear dynamics of the integrated energy system and the discrete operating decisions related to grid energy exchange and battery charge and discharge scheduling. In addition, the C-MPC strategy allows the forecast of the indoor temperature in building, the buffer tank temperature and battery state of charge through the dynamic behavior of the energy storages system. An accurate prediction of the outdoor temperature and the PV irradiance measurement was also incorporated. The MINLP-based C-MPC strategy was implemented in Python with the GEKKO library. Simulation results show an effective energy management between the different subsystems with a reduced energy consumption without compromising the occupant comfort. The proposed strategy increases PV-self consumption, reduces grid electricity use and improves efficiency of the surface water heat pump.

References

[1] International Energy Agency, "Buildings," 2024. [Online]. Available: https://www.iea.org/energy-system/buildings

[2] A. López-Ceballos, C. del Cañizo, I. Antón, and A. Datas, "Integrating lithium-ion and thermal batteries with heat pumps for enhanced photovoltaic self-consumption," *Appl. Energy*, vol. 390, 125767, 2025.

[3] Y. Wu, Z. Liu, B. Li, H. Liu, R. Liu, and L. Zhang, "Optimal storage capacity for building photovoltaic-energy storage systems considering energy flexibility management," *Energy Build.*, vol. 338, 115757, 2025.

[4] A. Rinaldi, M. C. Soini, K. Streicher, M. K. Patel, and D. Parra, "Decarbonising heat with optimal PV and storage investments: A detailed sector coupling modelling framework with flexible heat pump operation," *Appl. Energy*, vol. 282, 116110, 2021.

[5] L. Liu, S. Jiang, T. Jia, X. Li, Y. Zhao, and Y. Dai, "Numerical and experimental investigation on solar photovoltaic-thermal assisted heat pump systems using different kinds of solar cells," *Renew. Energy*, vol. 250, 123319, 2025.

[6] J. Salpakari and P. Lund, "Optimal and rule-based control strategies for energy flexibility in buildings with PV," *Appl. Energy*, vol. 161, pp. 425–436, 2016.

[7] J. Drgoňa, J. Arroyo, I. C. Figueroa, D. Blum, K. Arendt, D. Kim, E. P. Ollé, J. Oravec, M. Wetter, D. L. Vrabie *et al.*, "All you need to know about model predictive control for buildings," *Annu. Rev. Control*, vol. 50, pp. 190–232, 2020.

[8] P. Sawant, O. Villegas Mier, M. Schmidt, and J. Pfafferott, "Demonstration of optimal scheduling for a building heat pump system using economic-MPC," *Energies*, vol. 14, no. 23, 7953, 2021.

[9] C. Baumann, P. Wohlgenannt, W. Streicher, and P. Kepplinger, "Optimizing heat pump control in an NZEB via model predictive control and building simulation," *Energies*, vol. 18, no. 1, 100, 2024.

[10] F. Liberati, A. Di Giorgio, A. Giuseppi, A. Pietrabissa, E. Habib, and L. Martirano, "Joint model predictive control of electric and heating resources in a smart building," *IEEE Trans. Ind. Appl.*, vol. 55, no. 6, pp. 7015–7027, 2019.

[11] A. Parisio, E. Rikos, and L. Glielmo, "A model predictive control approach to microgrid operation optimization," *IEEE Trans. Control Syst. Technol.*, vol. 22, no. 5, pp. 1813–1827, 2014.

[12] I. Gomes, M. Ruano, and A. Ruano, "MILP-based model predictive control for home energy management systems: A real case study in Algarve, Portugal," *Energy Build.*, vol. 281, 112774, 2023.

[13] F. Bre and V. D. Fachinotti, "A computational multi-objective optimization method to improve energy efficiency and thermal comfort in dwellings," *Energy Build.*, vol. 154, pp. 283–294, 2017.

[14] P. H. Shaikh, N. B. M. Nor, P. Nallagownden, and I. Elamvazuthi, "Intelligent multi-objective optimization for building energy and comfort management," *J. King Saud Univ. Eng. Sci.*, vol. 30, no. 2, pp. 195–204, 2018.

[15] A.-M. Sigounis, C. Vallianos, and A. Athienitis, "Model predictive control of air-based building integrated PV/T systems for optimal HVAC integration," *Renew. Energy*, vol. 212, pp. 655–668, 2023.

[16] M. Mohammadi, Y. Noorollahi, B. Mohammadi-Ivatloo, and H. Yousefi, "Energy hub: From a model to a concept–A review," *Renew. Sustain. Energy Rev.*, vol. 80, pp. 1512–1527, 2017.

[17] H. Håkansson, "Model-based optimization of hydronic heating system operations enhancing comfort and energy efficiency in the existing building stock," Master's thesis, Chalmers Tekniska Hogskola (Sweden), 2025.

[18] M. De Carli, L. Odersky, E. Prataviera, S. Bordignon, A. Di Bella, A. Zarrella, M. Khajedehi, M. Vanzetto, and T. Hamacher, "A comparison between the software EUReCA and UrbanEnergyPro on a district in Germany," in *J. Phys. Conf. Ser.*, vol. 3143, no. 1. IOP Publishing, 2025, 012103.

[19] N. Koumbari, L. Tziovani, M. Asprou, L. Hadjidemetriou, and S. Timotheou, "Thermal dynamic models for predicting the indoor temperature of multi-zone buildings," in *Proc. Int. Conf. Smart Energy Syst. Technol.* IEEE, 2024, pp. 1–6.

[20] L. Beal, D. Hill, R. Martin, and J. Hedengren, "GEKKO optimization suite," *Processes*, vol. 6, no. 8, 106, 2018.

[21] WaterWarmth, "Waterwarmth project," 2026. [Online]. Available: https://www.interregnorthsea.eu/waterwarmth

[22] NASA, "NASA POWER - Data Access Viewer," 2026. [Online]. Available: https://power.larc.nasa.gov/data-access-viewer/